Precision Pointing Considerations for Long-Distance Free-Space Optical Communications

John Thomas Beasley, Thomas Benjamin Walsh, Eric Glenn Forstner
BEI Precision
1100 Murphy Drive, Maumelle, AR 72113, USA; 501-851-5450
john.beasley@beiprecision.com

ABSTRACT

Present and future demand for global, low-latency telecommunications gives rise to several proposed constellations of satellites in Low Earth Orbit that feature high-bandwidth optical network links between spacecraft.

Free-space optical communication between satellites on separate orbital planes is a non-trivial endeavor. Over long distances, the budget for pointing error is very restricted. To illustrate the scales involved, this paper begins with a quantitative examination of angular inter-satellite vectors. This establishes context for the subsequent presentation of relevant design, integration, and on-orbit considerations that affect the ultimate performance of extremely precise pointing and tracking systems.

Coarse pointing precision plays a substantial role in the link acquisition sequence, but opto-mechanical considerations are often underestimated. This can lead to trade studies that result in higher divergence and higher power acquisition systems. Adequate design of coarse pointing assemblies (CPA), leading to superior boresight accuracy, can relieve the pointing requirements on fine pointing assemblies (FPA). With lower FPA range requirements, similar dynamic range capabilities of FPA sensors result in higher resolution beam pointing. CPA precision trade studies will be performed on realistic inter-satellite link angles to examine error sources and highlight pitfalls.

INTRODUCTION AND BACKGROUND

Optical communications systems can be as simple as the number of lanterns visible in a landmark structure's tower, as widespread as today's IR remote controls for sending unidirectional commands to consumer electronics, and as complex as systems for communications with spacecraft exploring the far reaches of our solar system and beyond.[1, 2, 3]

In this paper, the term "optical" will refer to electromagnetic (EM) radiation including both the Infra-Red (IR) and visible frequency ranges of 0.3 to 400 terahertz (THz) and 400 THz to 800 THz, respectively. The paper will refer to the radio frequency (RF) range as extending from 300 kilohertz (kHz) up to 300 gigahertz (GHz).

The demand for high-capacity information transfer across the globe is ever growing. This growing demand has been satisfied over the years by an evolution of communications systems that have used progressively higher frequencies of EM radiation. Optical communications systems using optical fiber conduits have been developed and deployed for data links across Earth's surface. These form high-capacity channels carrying vast amounts of data for networked computer systems, such as the Internet. The next evolution of optical communications systems is underway – establishing data transfer through direct line-of-sight from sender to receiver terminals, without a dedicated optical transmission medium. These are generically called Free Space Optical Communications (FSOC) systems.

Lasers are optical sources that provide FSOCs significant advantages of high concentration of optical power, narrow spectral linewidth, and phase coherence. A common misconception exists that the optical bundle of a laser, or its beam, maintains a consistent width for as far as it travels. Reality is different. The minimum angular width (θ, *radians*) of transmitted EM energy is proportional to the ratio of its wavelength (λ) and the diameter (D) of the transmitting aperture by:[4, 5]

$$\theta \propto \lambda / D \tag{1}$$

This relationship reveals advantages and disadvantages to consider when performing trade studies of the frequency and aperture to use for particular communication purposes. If the goal is to provide a broad area broadcast, one might choose a longer wavelength EM radiation source and use a very small transmitting aperture. Conversely, if the goal is to achieve a highly directed or tightly focused communication channel, one might choose a shorter wavelength radiation and use a larger transmitting

aperture. This choice could apply if the goal is to minimize the physical size of the transmitter, reduce transmitter power, increase intensity at the receiver, improve data privacy, or to communicate across large distances,

These trades have been studied for decades and are still actively pursued today. Numerous studies have included a determination that FSOC laser terminals aboard spacecraft have lower mass, occupy less volume and require less power than RF systems capable of operating with similar data volumes.[5 - 11] However, the optimal EM source band for each mission or application may vary. For near Earth distances (< 10^8 km) and inter-satellite communications, the balance of favor has shifted in recent years towards the use of FSOC systems.

The benefits offered by FSOCs over RF communications systems come at the cost of having to point the optical transmitter terminal more accurately toward the intended optical receiver terminal. This means the transmitter must have knowledge of the relative direction of the receiver and a direct line-of-sight to it. To establish this relative direction between separate spacecraft, the transmitter must have knowledge of its own position and orientation and the expected positon of the receiver at a determined point in time.

The transmitting spacecraft may point its laser in a particular direction in various ways. It can host a laser whose output beam is in a fixed orientation on the spacecraft. This is known as body pointing. It requires a high degree of knowledge and control of the spacecraft orientation. Adjustments to the orientation of the spacecraft require the development of forces (torques) acting upon the rotational inertia of the entire spacecraft, not just that of the communication system. As such, these tend to have more difficulty rapidly adjusting their pointing than a lower-inertia subsystem aboard the spacecraft.

Alternatively, the laser output can be directed by hosting the laser as a payload on a mechanism with one or more degrees of rotational freedom. This mechanism will be referred to as a gimbal. A consequence of this approach is that it requires electrical power and the information data stream for the laser to be provided across one or more rotating interfaces. An approach that alleviates this requirement is to place the laser on an optical bench – with an orientation fixed relative to the body of the spacecraft – and then to use gimbaled reflective or refractive optical elements to redirect the output beam of the laser. The common feature of these approaches is the presence of a gimbal. The study of this paper applies to either of these approaches.

The task of directing the output beam of a laser system is often split into several functions. [4, 5] The first is to understand the position and orientation of the spacecraft body. The second is to use a coarse pointing assembly (CPA) to redirect the beam around a large range of angles – which could be a full hemisphere or more. [12, 13, 14] The third function is to make small adjustments to the beam direction with a low-mass and responsive fine pointing assembly (FPA) in order to compensate for vibrations affecting the spacecraft body or optical bench hosting the laser source.

Of particular interest for this paper are constellations of several to many individual spacecraft operating in Low Earth Orbit (LEO) each with the ability to establish one or more optical connections to other spacecraft and transfer data across large distances. These FSOC systems are categorized as Optical Inter-Satellite Links (OISLs). OISLs are a part of a larger category called Inter-Satellite Links (ISLs), which also includes RF communications (RF ISLs). OISLs provide the ability to establish networked bidirectional pathways for the purposes of high performance global communications.

While adoption of FSOC between spacecraft is not already widespread, numerous advancements, deployments, and demonstrated capabilities have occurred.[1, 7, 15, 11] Several plans for these constellations have attracted significant media attention. These constellations benefit from advantages offered by satellites in LEO (altitude of 160 km to 1000 km) as compared to satellites operating in Geostationary Orbit (altitude of $\approx$ 36,000 km), two of which are reduced launch energy required to reach orbit, and reduced temporal lag (latency) for signals travelling between Earth's surface and the satellite.

The highest profile of these is arguably the SpaceX Starlink constellation, which has caused much consternation among Earth-bound astronomers. Although it has been announced that this constellation will eventually include OISLs, publicly available information to date indicates that the initial batches of satellites deployed thus far do not contain them.[16] Each of thousands of spacecraft may eventually host four or even five OISL terminals.

Telesat LEO is another global broadband communications constellation planned to utilize OISLs. Evaluation of competing satellite designs is still underway. There are plans for 300 or more satellites, each with multiple OISL terminals.

The United States Defense Advanced Research Projects Agency has awarded contracts for systems to be tested on its Blackjack satellites. The successes of this program are planned to be the building blocks for the National Defense Space Architecture, envisioned to be a constellation comprised of hundreds to thousands of satellites.[17]

The European Space Agency, Airbus, the German Aerospace Center (DLR), and Tesat-Spacecom GmbH & Co. KG have established a history of successful optical links between geostationary orbiting EDRS satellites and four LEO Earth-observation spacecraft.

Other agencies with published articles or press releases about their advancements in OISLs for space applications include: Japan Aerospace Exploration Agency (JAXA), Australian Space Agency, Northrop Grumman, L3Harris Technologies, Mynaric, SA Photonics Inc., Massachusetts Institute of Technology (MIT), Advanced Technology Associates (ATA), The Aerospace Corporation, Space Micro, Inc., Fibertek Inc., and Facebook.

With OISL designs originating from many different organizations, groups are recognizing that advantages can be gained if interoperability between various systems could be achieved. Efforts to establish standardized design and operational parameters for OISLs are already underway. The Consultative Committee for Space Data Systems is formed from many member agencies and many more agencies that are observing. It has published recommendations to utilize optical wavelengths in the IR band near 1 μm and 1.55 μm.[18]

This standard calls for a two-staged approach to establishing an optical link, much like as has been described by other authors.[4] The first stage utilizes a "beacon" laser near 1 μm aboard satellite A to essentially announce the intent to establish a link. This initial part of the "acquisition" stage will normally involve a scanning search by the beacon transmitter in the expected direction of partner satellite B. When the partner's receiver detects beacon energy, its onboard sensors determine the direction of the beacon and respond with a returned output transmission to acknowledge the initiation and provide an indication of its current location. From this point on, each system works to improve the alignment of its output beam to the partner until criteria are met to begin data transfer.

The simulations presented in this paper will provide insight into specifications related to pointing performance that need to be developed in the design of gimbals for FSOC purposes. The paper will present numerical analysis of the direct line-of-sight (LOS) pointing, or link vectors, required between two spacecraft, both operating in Low Earth Orbit (LEO). The simulation will also examine the effect of angular sensor characteristics used on the LOS gimbals. Sensitivities of small perturbations of position and orientation will also be discussed as well as drawing some attention to insidious error sources for optical beam pointing systems aboard spacecraft, such as mechanical misalignments resulting from launch stresses.

A suite of MATLAB scripts were written to perform the numerical analysis of the coarse pointing simulations discussed herein. The simulation is comprised of three main processes: orbit definition and propagation for two spacecraft, link vector derivation from transmitter to receiver, and a simulation of the pointing performance based on angular sensor characteristics. The simulation lacks a great many details to be considered a realistic representation of achieving an OISL, and is simply a testbed for comparison of angular sensor technologies. A description of the orbital mechanics program, a 3-degree-of-freedom (3DOF) simulation, follows.

ORBITAL MECHANICS SIMULATION

Assuming that the modeled objects are rigid bodies, the equations that describe the translational motion of an object in orbit are well known. This simulation considers a massless point (our lasercom spacecraft) orbiting a massive point (Earth). The first order, ordinary differential equations that describe such motion are derived from Newton's second law of motion. The acceleration due to gravity experienced by the spacecraft is expressed as:

$$\ddot{r} = -G\frac{m}{r^2}\hat{r} = -\frac{\mu}{r^2}\hat{r} \tag{2}$$

Where r is the position vector of the spacecraft in the ECI coordinate frame, such that **r** = [X, Y, Z]. **G** is the universal gravitational constant, and m is the mass of the Earth, such that μ = G ·m is the standard Earth gravitational parameter (398600.4418 $\frac{km^3}{s^2}$). [19] Taking the gradient of the acceleration above allows for the orthogonal equations of motion (EOM) to be expressed extrinsically:

$$\ddot{X} = -\frac{\mu X}{r^2}\hat{r} \tag{3}$$

$$\ddot{Y} = -\frac{\mu Y}{r^2}\hat{r} \tag{4}$$

$$\ddot{Z} = -\frac{\mu Z}{r^2}\hat{r} \tag{5}$$

The use of these equations requires an inertial coordinate system such as the Earth Centered Inertial (ECI) coordinate frame.

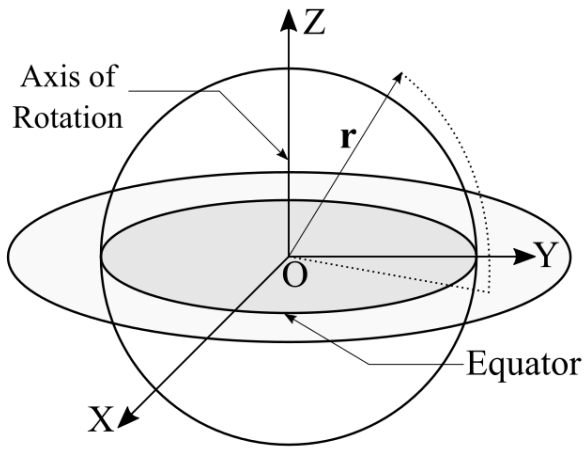

Figure 1: Earth Centered Inertial (ECI) Coordinate Frame

To add to the simulation's fidelity, gravitational perturbations describing an oblate spheroid are summed into the acceleration terms of the equations of motion. A full model of Earth's gravitational field can be described with Legendre polynomials; however, we will only sum the contribution from the J_2 zonal harmonic. The J_2 zonal harmonic describes the effect due to the Earth's bulging equator, and is a primary contributor to low Earth orbit perturbations. The gravitational potential is expressed as:

$$U_2 = -\frac{\mu J_2 R_e^2}{2}\left(\frac{3Z^2}{r^5} - \frac{1}{r^3}\right) \tag{6}$$

Here, J_2 is the zonal coefficient (-0.001082635854), R_e is the mean radius of the earth (6378.137 km), and Z refers to the coordinate in the ECI frame. Taking the gradient of U_2 expresses the acceleration terms to be added to the EOM accelerations:

$$\ddot{U}_{2,X} = \frac{\mu J_2 R_e^2}{2}\left(\frac{15Z^2X}{r^7} - \frac{3X}{r^5}\right) \tag{7}$$

$$\ddot{U}_{2,Y} = \frac{\mu J_2 R_e^2}{2}\left(\frac{15Z^2Y}{r^7} - \frac{3Y}{r^5}\right) \tag{8}$$

$$\ddot{U}_{2,Z} = \frac{\mu J_2 R_e^2}{2}\left(\frac{15Z^3}{r^7} - \frac{9X}{r^5}\right) \tag{9}$$

Now, with the definition of the orbital state vector

$$S = [X, Y, Z, V_X, V_Y, V_Z]^T \tag{10}$$

where V_X, V_Y, and V_Z are the orthogonal velocity components in the three ECI axes, we can express the EOMs as six first-order equations by taking the first derivative of S:

$$\dot{X} = V_X \tag{11}$$

$$\dot{Y} = V_Y \tag{12}$$

$$\dot{Z} = V_Z \tag{13}$$

$$\dot{V_X} = -\frac{\mu X}{r^2}\hat{r} + \ddot{U}_{2,X} \tag{14}$$

$$\dot{V_Y} = -\frac{\mu Y}{r^2}\hat{r} + \ddot{U}_{2,Y} \tag{15}$$

$$\dot{V_Z} = -\frac{\mu Z}{r^2}\hat{r} + \ddot{U}_{2,Z} \tag{16}$$

To complete the orbital mechanics simulation, these equations are numerically integrated with a fifth order Runge-Kutta scheme proposed by Dormand & Prince.[20] A fixed time step is used to generate a time array to propagate both the receiver and transmitter orbits. This produces synchronous position states to evaluate OISL vectors.

LINK VECTOR DERIVATION

The post-processing of spacecraft state vectors begins with the derivation of the transmitter's attitude rotation matrix. With the attitude and position state knowledge, gimbal angles (azimuth & elevation) are derived that point the transmitter aperture to the receiver. The attitude formalism used to define the spacecraft is consistent with a velocity, normal, co-normal orientation. The spacecraft principal reference frame $[\hat{x}_{SC}, \hat{y}_{SC}, \hat{z}_{SC}]$ is defined by:

$$\hat{x}_{SC} = \frac{v}{\|v\|} \tag{17}$$

$$\hat{y}_{SC} = \frac{r \times v}{\|r \times v\|} \tag{18}$$

$$\hat{z}_{SC} = \hat{x}_{SC} \times \hat{y}_{SC} \tag{19}$$

Where v is the velocity state vector $[V_X, V_Y, V_Z]$.

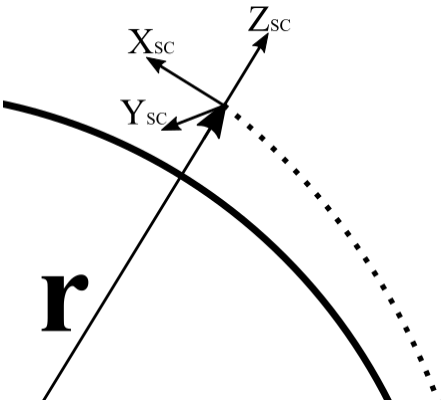

Figure 2: Spacecraft Attitude Formalism

This triad forms the 3x3 rotation matrix used to obtain the communications link vector in the transmitter's reference frame from the inertial frame.

$$R_{SC} = \begin{bmatrix} \hat{x}_{SC} \\ \hat{y}_{SC} \\ \hat{z}_{SC} \end{bmatrix} \tag{20}$$

The link vector $\boldsymbol{L}$, simply the subtraction of the receiver from the transmitter's position state, is rotated into the transmitter's body-fixed attitude frame (denoted with 'SC' subscript) by: $L_{SC} = R_{SC} \cdot L$. Position knowledge error of the receiver spacecraft is simulated by propagating its orbit with an initial spatial uncertainty of 100 meters. This rotated link vector is used to determine the gimbal azimuth and elevation angles that point directly at the receiver spacecraft, where $\boldsymbol{L}_{SC,X}$ denotes the product of the vector with a unit vector $\hat{\imath}$, $\hat{\jmath}$, or $\hat{k}$. The following calculations are performed twice in the simulation: once without any position knowledge error for comparison purposes, and once with position and attitude knowledge error for advancing through the simulation. Attitude knowledge error with a standard deviation of 30 μrad is summed with the result of the Azimuth and Elevation angle derivations below.

$$Azimuth = \psi = \tan^{-1}\frac{L_{SC,\hat{\jmath}}}{L_{SC,\hat{\imath}}} \tag{21}$$

$$Elevation = \theta = \tan^{-1}\frac{L_{SC,\hat{k}}}{\sqrt{L_{SC,\hat{\imath}}{}^2 + L_{SC,\hat{\jmath}}{}^2}} \tag{22}$$

GIMBAL POINTING SIMULATION

The final stage of the simulation is composed of a discrete time closed-loop PID control simulation of both azimuth and elevation axes of the CPA gimbal. The simulation employs two modes: acquisition and tracking. During acquisition, the feedback loop error term is the difference between the acquisition search point and the gimbal axis sensor, an output of the function *Sensor Map*.

The acquisition search point is a moving target that spirals in on the best-known location of the receiver spacecraft, the position that includes position and attitude knowledge error. The initial acquisition search point is equivalent to the initial best-known location plus a radial "cone of uncertainty" value calculated from link distance and a priori knowledge of spacecraft tracking limitations. For the purposes of this simulation, the value used is 134 μrad. This is derived from the 100 meter position uncertainty and the minimum link distance (resulting in 34 μrad) plus 100 μrad to account for the remainder of uncertainties generated from attitude and gimbal sensor error. From this initial point, the search point spirals in toward the best known receiver location. If the gimbal points toward the true receiver spacecraft location to within 25 μrad for 5 seconds, an acquisition is considered to be made. This can be considered the equivalent of a divergent beacon striking the receiver spacecraft wide field of view detector. If the gimbal does not locate the receiver spacecraft, the search spirals back out to the initial cone of uncertainty radius plus best known location. This repeats until the either the receiver spacecraft is located or the simulation ends.

The *Sensor Map* function adds repeatable angular error, quantization effects, and random noise to true gimbal angle to simulate the characteristics of different angular sensors. Repeatable error is added to the input angle as a Fourier sum of differing frequencies dependent upon input angle. Depending on device type, the amplitude and frequency of characteristic errors will differ. Furthermore, the number of series summed to create the error profile will vary to yield the intended device accuracy and characteristics. The routine also adds noise drawn from a Gaussian distribution that is characteristic of the device's Effective Number of Bits (ENOB). ENOB is defined as the standard deviation of the Gaussian noise expressed in bits of a full revolution. For example, an ENOB of 24 bits equates to: $\sigma_{noise} = \frac{2 \cdot \pi \ radians}{2^{24}} = 0.3745x10^{-6} \ radians$. Prior to output of the simulated device angle, the value is quantized to the sensor's resolution level.

Table 1: Rotary Sensor Performance Characteristics

Manufacturer	Sensor	Full Rev. Error (µrad RMS)	Interpolated Error (µrad RMS)	ENOB (bits)	Quanta (bits)
BEI Precision	nanoSeries ARA	<4.848	0.5	26	28
BEI Precision	nanoSeries TRACKER	<12	3	24	24
BEI Precision	nanoSeries MKE	<145	30	18	24
Theoretical	20 Bit Optical Encoder	53	12.5	20	20
Theoretical	16 Bit Optical Encoder	60	30	20	16
Theoretical	16 Bit Resolver	105	72	19	16

The above table lists the sensor options explored and their corresponding performance characteristics.

After acquisition, the receiver spacecraft position relative to the gimbal pointing vector can be relayed (through a return optical or RF link) back to the transmitter spacecraft for promotion of the control loop to tracking mode. During this mode, the acquisition search position is replaced by the true location of the receiver spacecraft. The control loop will maintain the optical link to the precision allowed by the gimbal angular sensors. It is worth noting again that the simulation lacks injection of vibration, receiver detector errors, or other link perturbations. The link tracking precision is an optimistic view of what actual CPA implementations can achieve.

SIMULATION RESULTS

For coarse pointing assemblies, beacon pointing accuracy drives the necessary divergence and power of the beacon laser. Since improving the accuracy of beacon pointing pays off with a quadratic gain in throughput, whereas increasing the beacon power only yields linear returns, rotary sensor choice is of utmost importance in CPA design.[21] A comparison of the different sensors listed in Table 1 will show the effects accuracy and quantization have on OISL tracking performance.

The chosen reference orbits with which the transmitter and receiver spacecraft follow are from no particular OISL mission. They are similar to the originally planned SpaceX Starlink constellation at altitudes of 1150 km.[22] The orbital elements of the transmitter spacecraft are listed below along with the receiver spacecraft differences in right ascension of the ascending node (R.A.A.N.) and true anomaly. Figure 3 depicts the ground track of both spacecraft with the OISL vector for one full orbit.

Table 2: Orbital Elements

Altitude	Eccentricity	Inclination	R.A.A.N.	Arg. of Perigee	True Anomaly	ΔR.A.A.N.	ΔTrue Anomaly
1000 km	.000125	50°	0°	0°	0°	20°	10°

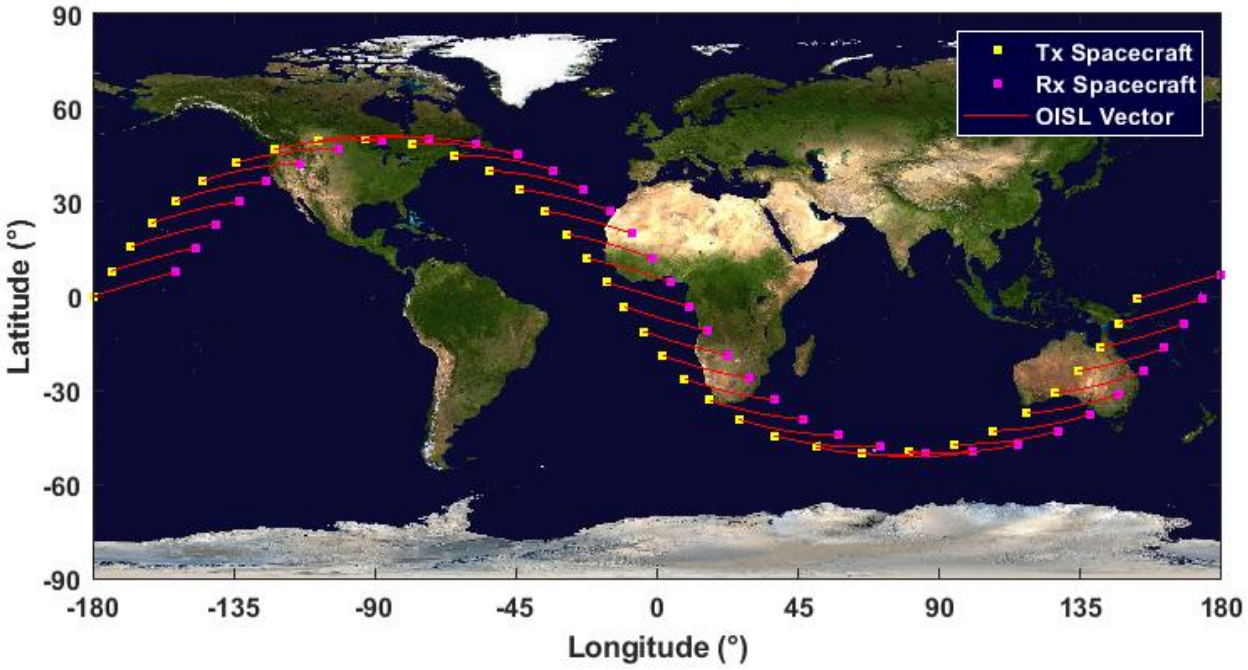

Figure 3: Ground Track of Tx/Rx Spacecraft

The link distance for the spacecraft pair is depicted in Figure 4, varying from nearly 2900 km to 3500 km.

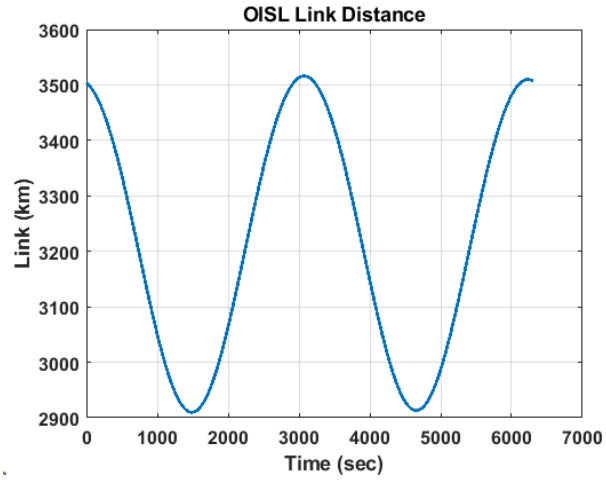

Figure 4: Link Distance

The gimbal pointing angles required to maintain the link are depicted in Figure 5. These are relative to the transmitter spacecraft's reference frame described previously.

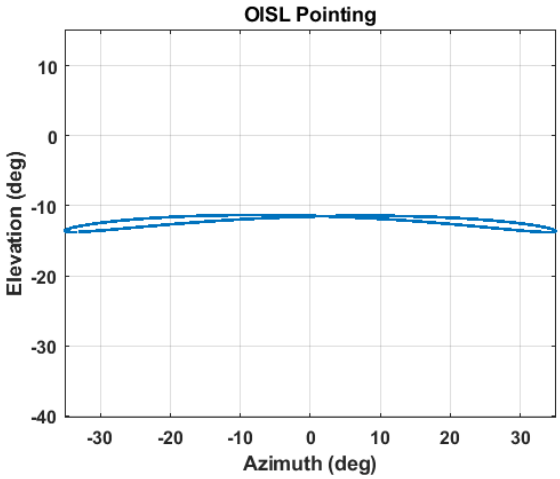

Figure 5: OISL Pointing Angles

Note that the azimuth pointing requirement varies much more than the elevation; this will become apparent in the disparity of the two sensor's performance discussed later. Further adding to the disparity are the required angular velocities to maintain tracking. Figure 6 depicts the ~10X difference in azimuth versus elevation tracking rates.

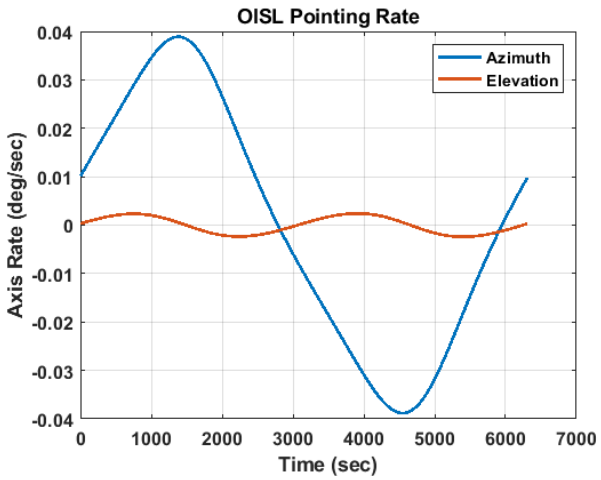

Figure 6: OISL Pointing Rates

The first comparison is made between sensors in the control-loop acquisition mode. Recall that once acquisition is made, the loop switches to tracking mode and tracks the actual receiver spacecraft position. Acquisition mode is depicted by the blue trace, and trace turns green once tracking mode is activated in Figure 7. Notice that the spiral search pattern can be easily seen with the higher precision angular sensors.

Figure 7 depicts that the search pattern is somewhat meaningless for lower precision sensors. The highly quantized or low accuracy sensors, such as MKE, do not have the precision required to maintain disparity between subsequent spiral passes. As such, there is a strong factor of luck in acquiring the target for these systems. Obviously, a much higher divergence beacon than the one simulated here would be needed for meaningful search patterns.

During tracking mode, the 16-Bit sensors maintain a modest tracking precision compared to the lower accuracy MKE and Resolver solutions. However, the coarse level of quantization limits the gimbal's ability to track the rapidly changing search pattern. Even with no repeatable error, a 16-bit sensor will provide substantial inaccuracies due to quantization.

The accuracy and precision of the ARA, TRACKER, and 20 Bit sensors is apparent in the fidelity with which the spiral search pattern is executed. This is echoed in the lower acquisition time and lower tracking jitter thereafter. The ARA optical encoder, BEI Precision's highest accuracy space sensor offering, is capable of sub-μrad pointing precision over limited angles. A reminder again that this simulation is negligent of vibration. In general, it is clear that the limited angular span and lower pointing rate of the elevation axis leads to better tracking performance, aside from any static offset.

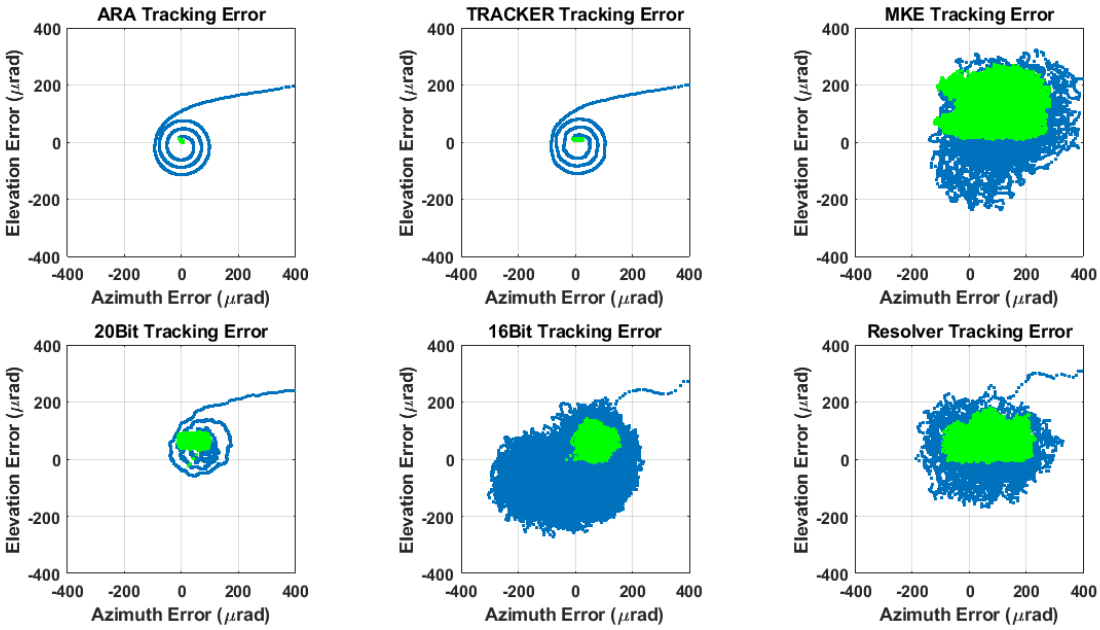

Figure 7: OISL Acquisition to Tracking Transition, All Sensors

Table 3: Acquisition Time & Tracking Accuracy

Sensor:	ARA	TRACKER	MKE	20Bit	16Bit	Resolver
Acquisition Time (sec)	91.5	93.0	2226.9	171.5	4288.4	1055.7
Az. Jitter after Acquisition (1-σ μrad)	1.176	5.559	71.942	24.163	21.123	58.520
El. Jitter after Acquisition (1-σ μrad)	0.514	1.437	61.647	11.282	24.038	29.877

A closer look at the ARA and TRACKER solution's tracking with 40 μrad axis limits shows the performance in higher detail. The disparity between azimuth and elevation can be clearly seen as the resulting error shape is somewhat rectangular. Also apparent is the DC offset for both axes corresponding to the error of the sensors. In practice, these offsets would need to be accounted for at this or the Fine Pointing Assembly level to achieve the best possible link. The precision of the ARA system is shown at least an order of magnitude better than 20 Bit or lower resolution sensors. With such improvement, the range required for Fine Pointing Assemblies can be reduced similarly, thereby enhancing the final pointing resolution of the system.

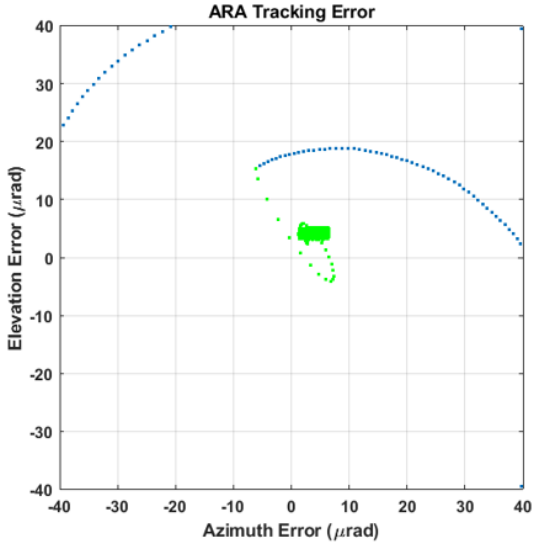

Figure 8: ARA Tracking Detail

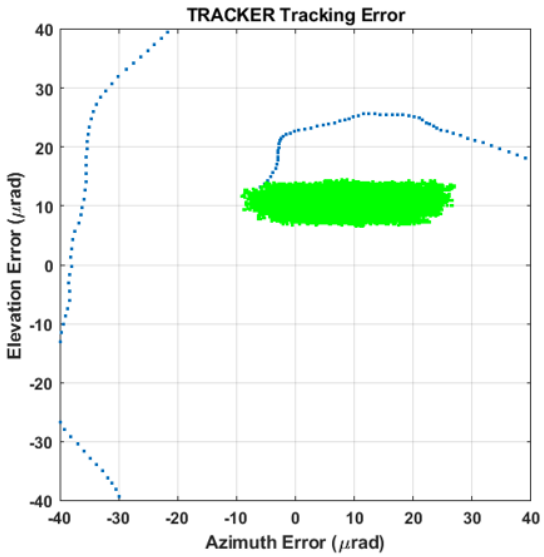

Figure 9: TRACKER Tracking Detail

Two insidious sources of error that can play a large role in OISL pointing precision are perturbations in the axis-of-rotation of one or both gimbal axes and the resulting errors from angular sensor misalignment. For single readstation optical encoders and resolvers, the centration of the rotor component is linearly proportional with a corresponding error term. A change in the location of the axis-of-rotation yields both this first-order error and others due to distortion of the interpolated position, especially in optical encoders that rely upon exacting optical alignment and calibration to report highly interpolated angular positions. A secondary effect other than the resulting sensor error is the introduction of a bias between the sensor's boresight position and the gimbaled optic. Such a perturbation would necessitate further on-orbit calibration. Consequently, in-situ knowledge of axis-of-rotation characteristics can be highly valuable to both on-orbit calibration schemes and would-be troubleshooters. BEI Precision nanoSeries encoders are equipped with *Alignment Mode*, the ability to report variations in the axis-of-rotation (both bias and runout) with respect to the stator mounted readstation. This feature not only aids in the rapid alignment of the encoder during installation, but also in spindle health monitoring throughout the mission.

Axis-of-rotation perturbations can manifest as any combination of a permanent shift or change in spindle runout. This can be due to the rigors of launch or environmental variations. [21] For sensors without the ability to correct for runout variation, the resulting error could render a CPA inadequate for acquiring targets. As an example, let's assume the azimuth axis of a CPA equipped with single readstation TRACKER encoders develops a 100 µrad 1st harmonic error due to unexpected axis runout, a mere increase of 0.0002" of total runout for a 4" code disk. This results in the system's inability to acquire the receiver spacecraft for over 1500 seconds in the baseline simulation. Additionally, the tracking ability thereafter is drastically reduced– see Figure 10. Two readstation TRACKER implementations would be robust against such position reporting errors, but would still suffer from reduced interpolation accuracy and any associated boresight shift. While boresight shifts are recoverable by most systems through on-orbit calibration, only angular sensors such as TRACKER (or other BEI Precision sensors) that can recalibrate in-situ can recover from the loss of interpolation accuracy.

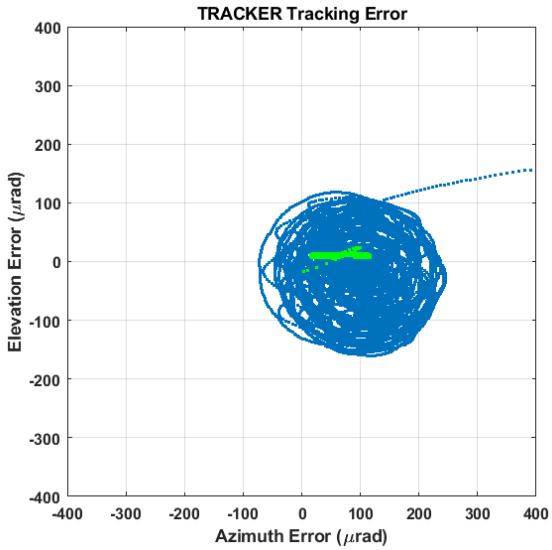

Figure 10: TRACKER System with Impaired Runout

Another scenario considered is the error due to a misaligned sensor after an axis-of-rotation shift. Even if the proportional error is nulled by having dual readstations and the boresight remains the same, the interpolated error can increase by an order of magnitude for modest misalignments. Figure 11 depicts such an error on the azimuth axis for an ARA equipped CPA.

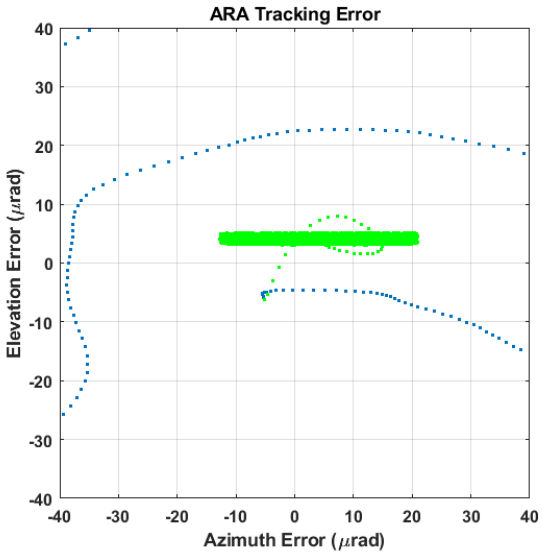

Figure 11: ARA System with Impaired Alignment, Before Calibration

The tracking inaccuracy, disregarding the bias, increased to 8.5 µrad. The only mechanism for recovery from this error type is recalibration of the angular sensor. Were it not for alignment reporting from the encoder, the host might be unaware of a change in the axis-of-rotation.

CPA DESIGN CONSIDERATIONS

Early design decisions in hierarchized assemblies can drive difficult requirements for the subassemblies downstream. For pointing assemblies, a decision at the CPA level can define requirements for the fine pointing assembly, beacon, and communication beam.

Apparent from the simulation scenarios is the need to establish axes-of-rotation that remain constant throughout time and environmental exposure. While many spindle designers strive for low torque and low runout, it is also critical to achieve high stiffness. This reduces variability through launch and into the weightless environment, maintaining angular sensor accuracy. For designers utilizing preloaded ball bearing pairs, this often means using back-to-back arrangements at the cost of higher running torque. Flexure based axes are of particular concern due to their tendency to deviate from true center as rotation occurs. Special attention should be paid to minimize non-rotary motion in these designs. Furthermore, installation of angular sensors should be as close as possible to the stiffest rotary joint to limit deflections.

Previous developments at BEI Precision have led to the axis motion measurement technique *Alignment Mode*. This feature, standard on all nanoSeries encoders, measures the distance from the center of the code disk to

the readstation in a relative sense. The output is signed, where the zero point is perfect alignment of the code disk and the optical feature, or grating, on the readstation. The response from *Alignment Mode* immediately after installation is based on the centering of the code disk and the alignment of the readstation to the perfect design radius. Any variation from this initial response will be caused by relative motion between rotor and stator of the spindle assembly, including relative thermal expansion between the code disk and readstation. This feature allows host systems to gain knowledge of axis-of-rotation shifts or changes in runout. It can be insightful during the development of flexural pivots, allowing the host to measure motion of an optical payload that is orthogonal to the axis (i.e. piston motion). Indication of axis shift would also raise concern about boresight accuracy and alignment.

Boresight bias, axes alignment, and sensor errors that arise from launch stress have to be accounted for during this phase. These sensor interpolation errors are often underestimated, but must be addressed for the most precise pointing applications. [23] Since no mechanism is infinitely stiff, inevitable axis-of-rotation variation will cause some amount of sensor alignment error that results in interpolation error. In lieu of relying on mechanism operators to derive truth maps for angular sensor outputs, an automatic calibration scheme is employed on BEI Precision nanoSeries encoders. Auto-Calibration is a command-able feature that tunes the underlying sinusoidal position signals generated from the encoder code disk. Mapping the sinusoidal signal irregularities, instead of the position output error, leads to an intrinsically accurate position. The errors inherent in sinusoids (bias, amplitude, phase, harmonic distortion) are well understood and readily controlled. The bias and amplitude of encoder sinusoids, once matched, remain constant through code disk illumination control. Phase and harmonic distortion remain constant once a mechanical equilibrium is established; mapping to internally generated references for these errors is effective.

CONCLUSION

Pointing mechanisms are one of the enabling technologies for optical inter-satellite communication links. Performance for these mechanisms is exacting, leading to complex designs requiring complex trade studies. This paper attempts to expand some understanding of the pitfalls and error sources associated with the rotational joints comprising a coarse pointing assembly. A simulation of inter-satellite link kinematics provides a test bed to explore performance parameters of various angular sensors. We have shown that the precision of the angular sensors onboard a CPA can drive many requirements in the acquisition phase of an OISL, and can potentially enhance OISL performance by alleviating the pointing requirements of the fine pointing assembly. Furthermore, key technologies such as Alignment Mode and Auto-Calibration can provide a valuable contingency for mission planners.

REFERENCES

1. H. Hemmati, A. Biswas and I. B. Djordjevic, "Deep-Space Optical Communications: Future Perspectives and Applications," Proceedings of the IEEE, vol. 99, no. 11, pp. 2020-2039, 2011
2. D. Boroson, "On achieving high performance optical communications from very deep space [10524-11]," in Proceedings of the SPIE 10524, Free-Space Laser Communication and Atmospheric Propagation XXX, San Francisco, CA, USA, 2018.
3. B. G. Boone, R. L. McNutt Jr., A. Mubashir, A. L. Beck, M. Edaibat, K. Kufahl and R. R. Shaw, "Quantitative evaluation of a dual-band spacecraft communication concept for a 1000 AU interstellar pathfinder mission," in Proc. SPIE 10910, Free-Space Laser Communications XXXI, 1091003, San Francisco, California, United States, 2019.
4. D. G. Aviv, Laser Space Communications, Norwood, MA, Massachusetts: Artech House, 2006.
5. W. Leeb, "Space Laser Communications: Systems, Technologies, and Applications," *The Review of Laser Engineering*, vol. 28, pp. 804-808, 2000.
6. K. Wilson and M. Enoch, "Optical Communications for Deep Space Missions," *IEEE Communications Magazine*, pp. 134-139, August 2000.
7. M. Toyoshima, "Trends in satellite communications and the role of optical free-space communications," *Journal of Optical Networking*, vol. 4, no. 6, pp. 300-311, 2005.
8. W. D. Williams, M. Collins, D. M. Boroson, J. Lash, A. Biswas, R. Orr, L. Schuchman and O. S. Sands, "RF and Optical Communications: A Comparison of High Data Rate Returns From Deep Space in the 2020 Timeframe," NASA STI Program, NASA Langley Research Center, Hampton, VA 23681-2199 USA, 2007.
9. M. Toyoshima, W. R. Leeb, H. Kunimori and T. Takano, "Comparison of microwave and light wave communication systems in space applications," *Optical Engineering*, vol. 46, no. 1, January 2007.
10. B. Moison and W. Farr, "Range Dependence of the Optical Communnications Channel," *IPN Progress Report*, vol. 42, no. 199, pp. 1-10, 2014.
11. H. Kaushal and G. Kaddoum, "Optical Communication in Space: Challenges and

Mitigation Techniques," *IEEE Communications Surveys & Tutorials*, vol. 19, no. 1, pp. 57-96, 2017.

12. A. Seas, B. Robinson, T. Shih, F. Khatri and M. Brumfield, "Optical Communications Systems for NASA's Human Space Flight Missions," in *International Conference on Space Optics (ICSO) 2018*, Chania; Greece, 2018.
13. T. Shih, C. DeVoe, O. Guldner, W. Hubbard, F. Khatri, S. Constantine, J. W. Burnside, J. Torres and B. S. Robinson, "A modular, agile, scalable optical terminal architecture for space communications," in *2017 IEEE International Conference on Space Optical systems and Applications (ICSOS)*, Naha, Japan, 2017.
14. K. Nakagawa and A. Yamamoto, "Preliminary design of Laser Utilizing Communications Equipment (LUCE) installed on Optical Inter-Orbit Communications Engineering Test Satellite (OICETS)," in *Proc. SPIE 2381, Free-Space Laser Communication Technologies VII*, San Jose, CA, USA, 1995.
15. A. A. Kazemi, "High Speed Laser Based Intersatellite Link Systems for Harsh Environment of Space," *Advances in Theoretical & Computational Physics*, vol. 2, no. 1, pp. 1-8, 2019.
16. S. Erwin, "U.S. Army signs deal with SpaceX to assess Starlink broadband," 26 May 2020. [Online]. Available: https://spacenews.com/u-s-army-signs-deal-with-spacex-to-assess-starlink-broadband/. [Accessed 8 June 2020].
17. S. Erwin, "DoD to test laser communications terminals in low Earth orbit," 8 June 2020. [Online]. Available: https://spacenews.com/dod-to-test-laser-communications-terminals-in-low-earth-orbit/. [Accessed 8 June 2020].
18. The Consultative Committee for Space Data Systems, "Recommended Standard for Optical Communications Physical Layer CCSDS 141.0-B-1," CCSDS Secretariat, National Aeronautics and Space Administration, Washington, D.C. USA, 2019.
19. O. Montenbruck and E. Gill, Satellite Orbits: Models, Methods, & Applications, Berlin: Springer, 2000.
20. J. R. Dormand and P. J. Prince, "A Family of Embedded Runge-Kutta Formulae," *Journal of Computational and Applied Mathematics*, vol. 6, no. 1, pp. 19-26, 1980.
21. K. M. Reising, *Development of a Pointing, Acquisition, and Tracking System for a Nanosatellite Laser Communications Module (M.S. Thesis)*, Cambridge, MA: Dept. of Aeronautics and Astronautics, Massachusetts Institute of Technology, 2015.
22. A. G. Elias, C. T. Ribera, S. R. Cachafeiro and L. Bouyeron, "Encoder In-Orbit Calibration of the MTG Scanner," in *Proc. ESMATS 2017*, Univ. of Hertfordshire, Hatfield, U.K., 2017.